Transition of eruptive style: Pumice raft to dome-forming eruption at the Havre submarine volcano, South Pacific Ocean

Michael Manga[1], Samuel J. Mitchell[2], Wim Degruyter[3], and Rebecca J. Carey[4]

[1]Department of Earth and Planetary Science, University of California, Berkeley, California 94720, USA

[2]Department of Geology and Geophysics, University of Hawai'i at Manoa, Honolulu, Hawaii 96822, USA

[3]School of Earth and Ocean Sciences, Cardiff University, Cardiff CF10 3AT, Wales, UK

[4]School of Earth Sciences, University of Tasmania, Hobart, Tasmania 7001, Australia

ABSTRACT

Transitions in eruptive style are common at volcanoes. Understanding how and why these transitions occur remain open questions. The 2012 eruption of the submarine Havre volcano in the Kermadec arc (South Pacific Ocean) produced a raft of floating pumice followed by a pair of domes from the same vent. Here, we used measurements on erupted magmas and constraints on the eruption rate, combined with a model for magma ascent, to identify the dominant controls on the transition in eruption style. During the raft-forming stage, magma ascent was fast enough that little gas was lost. Magma reached the seafloor with great enough vesicularity to be buoyant and produce clasts that could float. As the eruption waned, the eruption rate decreased and the conduit narrowed. Sufficient gas was then lost to the surrounding country rocks during ascent such that the erupted magma was no longer buoyant relative to seawater. Most of the original

dissolved water in the magma was lost to the crust surrounding the conduit during the dome-forming stage.

INTRODUCTION

Volcanic eruptions commonly transition between different styles, for example between explosive and effusive eruption. Understanding how and why these transitions occur remain key outstanding questions (National Academies of Sciences, Engineering, and Medicine, 2017) that provide insight into both ascent processes and hazards (Cassidy et al., 2018). The 2012 silicic submarine eruption of Havre volcano in the Kermadec arc, South Pacific Ocean (Fig. 1A) provides a new opportunity to understand transitions in eruptive style. Initially, it created a gigantic raft of floating pumice (Fig. 1B; Jutzeler et al., 2014) and then it extruded a dome on the seafloor from the same vent, 900 m below sea level (Fig. 1C; Carey et al., 2018).

Here we used a model for magma ascent in a conduit, constrained by measured magma properties, seafloor observations, and eruption constraints, to elucidate the processes governing eruption style. We propose that as the eruption rate decreased during the course of the eruption, sufficient gas loss during ascent eventually led to magma erupting on the seafloor with vesicularities low enough to be denser than seawater and hence to form a dome.

THE 2012 HAVRE ERUPTION

The 2012 Havre eruption was the largest deep silicic submarine eruption recorded since A.D. 1650 (Jutzeler et al., 2014). On July 18, 2012, more than 1.2 km^3 of pumice (bulk volume) reached the ocean surface (Carey et al., 2018), creating a raft of pumice

45 that floated for years and distributed pumice around the Pacific and Southern Ocean
46 basins (Jutzeler et al., 2014).
47 In March 2015, to better understand this eruption, the Mapping Exploration and
48 Sampling of Havre (MESH) expedition made a high-resolution (1-m resolution)
49 bathymetric map (Fig. 1C) and collected 290 samples from different locations on the
50 submarine edifice. Submarine exploration of the volcano revealed three clastic
51 pumiceous units, and 15 domes and lavas (Carey et al., 2018). Mapping of stratigraphic
52 relationships and sampling demonstrated that the vent responsible for the pumice raft is
53 overlain by a 250-m-high, 0.11 km^3 pair of domes also erupted in 2012, which we refer to
54 as the OP dome (Fig. 1C). The OP Dome is unusual in that it is offset from the structural
55 lineament parallel to the southern caldera margin that focused magma in seven other
56 locations to form smaller domes (Fig. 1).
57 The creation of pumice clasts in subaerial settings is generally attributed to the
58 fragmentation processes that lead to an explosive eruption. Manga et al. (2018) showed
59 that the high hydrostatic pressure at the vent allowed sufficient water to remain dissolved
60 in the melt such that the magma viscosity was too low to permit brittle fragmentation in
61 the conduit, and the resulting pumice raft-forming eruption was effusive. Furthermore,
62 Manga et al. (2018) proposed that buoyant magma was extruded into the ocean where it
63 fragmented upon quenching (van Otterloo et al., 2015) and was then able to float to the
64 ocean surface to supply the pumice raft (Fauria and Manga, 2018).
65 There remains a key open question: why did the extruded magma change from
66 being less to more dense than ocean water? The compositions of dome OP and raft
67 pumice are essentially identical (Table DR1 in the Supplementary Material). The main
68 obvious differences are the vesicularity and texture (Fig. 2): Raft pumice has a mean

vesicularity of 78% (Rotella et al., 2015; Carey et al., 2018) and the average of 36 samples from the dome carapace and talus is 38.9% (Table DR2). While the vesicles are filled with gas, pumice and dome clast densities are less and greater than that of seawater, respectively. The irregular-shaped vesicles in the dome samples (Fig. 2B) suggest gas loss and collapse.

ASCENT MODEL

We consider a one-dimensional isothermal and quasi-steady model for magma ascent through a cylindrical conduit of constant radius *r* following Kozono and Koyaguchi (2012). Two-dimensional models (e.g., Chevalier et al., 2017) permit lateral variations in properties but show qualitatively similar results. Because the phenocryst volume fraction is low, ~5% (Carey et al., 2018), we consider two phases, melt and exsolved water with volume fraction ϕ, and use subscripts l and g to denote these two phases. We ignore crystallization during ascent, which would act to increase magma viscosity. The mass concentration of dissolved volatiles is c. We allow the melt velocity u_l and gas velocity u_g to differ, and we permit lateral gas loss through the conduit walls with flux Q_w. Conservation of mass for the melt and gas are, respectively,

$$\frac{d}{dz}[\rho_l(1-c)(1-\phi)u_l] = 0 \quad (1)$$

$$\frac{d}{dz}\left[\rho_l c(1-\phi)u_l + \rho_g \phi u_g\right] = -Q_w \quad (2)$$

where z is depth. Conservation of momentum, with inertial terms neglected owing to the low Reynolds number, is

$$0 = (1-\phi)\frac{dP}{dz} + \rho_l(1-\phi)g + F_{lw} \quad (3)$$

$$0 = \phi\frac{dP}{dz} + \rho_g \phi g + F_{lg} \quad (4)$$

where g is gravity and F_{lw} and F_{lg} describe the drag forces between magma and the conduit walls and between gas and liquid, respectively. The pressure P is assumed to be the same in the gas and melt.

We assume equilibrium outgassing with solubility given by

$$c = s\sqrt{P}\,. \tag{5}$$

We assume Poiseuille flow of the magma and thus

$$F_{lw} = \frac{8\mu}{r^2} u_l\,, \tag{6}$$

and vertical gas loss described by Darcy's law

$$F_{lg} = \frac{\mu_g}{k}\phi^2\left(u_g - u_l\right), \tag{7}$$

with permeability $k = 10^{-11}\phi^3$ m^2 (Mueller et al., 2005). Lateral gas loss through the conduit walls is driven by the pressure difference between magma in the conduit P and lithostatic pressure P_l in the surrounding crust (e.g., Jaupart and Allègre, 1991):

$$Q_w = \frac{2\rho_g \phi k_w}{\mu_g r^2}\left[P - P_l\right], \tag{8}$$

and it is 0 otherwise, with k_w being the country rock permeability. These models for vertical and lateral volatile loss ignore thermal, multiphase (e.g., liquid vs vapor), and turbulent effects. The viscosity of the magma μ_m varies with dissolved water content, which affects the melt viscosity μ_l (Manga et al., 2018), and ϕ (Llewellin and Manga, 2005), such that

$$\mu_m = \left(1 - \phi^{\frac{5}{3}}\right)\mu_l\,. \tag{9}$$

As boundary conditions, we specify the pressure at the vent (equal to the hydrostatic value at the seafloor depth of 0.9 km) and the mass inflow rate q at the bottom of the conduit. We use $c_0 = 4.9$ wt % based on melt inclusions from seafloor and raft

pumice (mean of 38 inclusions, standard deviation of 0.4 wt.%; summarized in Table DR3), temperature T = 850 °C (Manga et al., 2018), and $\rho_l = 2400$ kg/m^3, which is also assumed equal to the crust density, and μ_m. μ_l is a function of c, calculated using data from Giordano et al. (2008) for the composition and temperature reported in Manga et al. (2018). We solve for four depth-dependent variables, $P(z), \phi(z), u_l(z),$ and $u_g(z)$ in addition to the "chamber" pressure P_{ch} at the bottom of the conduit. Those variables also determine magma properties such as $\rho_g = P/RT$. We assumed a 5-km-long conduit and solve the coupled differential equations on a regular grid with 5 m spacing (parameters are summarized in Tables DR4).

RESULTS

Figure 3 shows the relationship between the mass eruption rate and vesicularity at the vent. We chose these two variables because they are measured (vesicularity) or bounded by observations (eruption rate) for the raft- and dome-forming stages (Carey et al., 2018). We considered two different conduit radii r = 30 m and 12 m, and three different wall-rock permeabilities, $k_w = 10^{-14}$, 10^{-13} and 10^{-12} m^2, to cover the range typical of upper crustal rocks (Manning and Ingebritsen, 1999) and oceanic crust (Fisher, 1998).

As the mass eruption rate increases, less gas is lost to the country rock, illustrating "the essential result that the fraction of gas lost is inversely proportional to the eruption rate because the flow of gas occurs at a given rate through the immobile country rock whilst magma rises" (Jaupart and Allègre, 1991, p. 416). At the lowest mass eruption rates shown, vertical gas loss can also reduce vesicularity even when the crust has a low permeability. However, to achieve vesicularities similar to those of the dome without

lateral gas loss, eruption rates are required that are a couple orders of magnitude lower than those calculated at Havre or recorded elsewhere, demonstrating that gas loss to the country rock must have occurred during ascent, and that lateral gas loss (controlled by country rock permeability) likely dominated over vertical gas loss (controlled by magma permeability).

As the conduit radius decreases, the amount of gas lost from the conduit increases. This occurs for two reasons. First, gas flux is inversely proportional to the square of conduit radius (Eq. 8). Second, as conduit size decreases, for the same mass flux, the resistance to ascent (Eq. 6) increases, leading to greater chamber and conduit pressures (colors in Fig. 3) and hence larger pressure differences driving lateral gas loss (Fig. DR5). Vesicularity can increase rapidly as magma approaches the vent owing to both a reduction in the pressure difference between the magma and its surroundings and the increasing ascent speed, which limits the time available for gas loss.

DISCUSSION AND CONCLUSIONS

During the course of an eruption, we expect the overpressure in the magma source to progressively decrease as magma is evacuated (e.g., Woods and Koyaguchi, 1994), leading to a decreasing mass eruption rate. Conduit size can also evolve: Conduit erosion acts to widen ascent paths, but decreasing pressure allows conduits to narrow (e.g., Costa et al., 2007) and cooling and/or crystallization of ascending magma near conduit walls may further decrease the effective conduit size. We ascribe the transition in eruption style at Havre volcano to both evolving magma pressure and decreasing conduit radius. The conduit size was largest during the pumice raft-forming stage of the 2012 Havre eruption, and minimal gas loss occurred during magma ascent because the ascent speed was too

high. As the eruption waned, the conduit narrowed, and vertical and lateral gas loss was enhanced.

There are a number of idealizations in the models and uncertainties in the eruption rate data used as inputs. Approximations in our model include a constant permeability for the crust, a cylindrical conduit, and neglect of crystallization. The conduit during the earliest phase of the eruption may well have been more elongate or dike-like, with a shape that evolved over the course of the eruption (e.g., Aravena et al., 2018), but there are no observations to better constrain vent and conduit geometry. The pumice raft samples have a very low abundance of microlites whereas dome samples have abundant microlites (Fig. 2) that nucleated and grew at some point during ascent or upon emplacement. The eruption rates plotted in Figure 3 are estimates from Carey et al. (2018) based on the mass erupted, constraints on the duration of eruption for the raft, and a lower bound for Dome OP based on 90 d between the raft-forming stage, 18 July 2012, and a comparison of bathymetric surveys on 17 October 2012 and March 2015 that revealed no further growth. This lower bound is within an order of magnitude of the mass eruption rates of recent small-volume rhyolite eruptions at Chaitén and Cordón Caulle (Pallister et al., 2013; Schipper et al., 2013; Tuffen et al., 2013) but considerably less than inferred rates for large-volume rhyolite flows (Befus et al., 2015). The eruption rate might also have decreased monotonically between these estimates for the raft and dome. Nevertheless, the general conclusion that increased gas loss occurs as eruption rate decreases should be robust. A decrease in radius of a factor of ~2 combined with a reasonable wall-rock permeability of $\sim 10^{-13}$ m^2 capture the observed vesicularities and estimates of mass eruption rates. Alternatively, an increasing permeability from 10^{-13} to

10^{-12} m^2, via fractures in the country rock or volcaniclastic layers, would also explain the changes in vesicularity. We also note that modest vesiculation may have continued as clasts rose in the water column above the vent, increasing raft vesicularity relative to the values at the vent (Mitchell et al., 2018), which are plotted in Figure 3.

Our explanation for the transition in eruption style requires large volatile fluxes through the magma, particularly during the dome-forming stage. Lateral volatile loss from the conduit to the surrounding rocks is a substantial fraction of the total magmatic volatile budget, ~25% and 70% of the initial water during the raft- and dome-forming stages, respectively (Fig. 3A). Further evidence for high exsolved volatile flux includes the presence of cristobalite in the dome samples (Fig. 2), which likely resulted from vapor-phase crystallization (e.g., Schipper et al., 2017). Given the initial water content of 4.9 wt% and erupted mass of the pumice raft and Dome OP, these values correspond to 5.4×10^9 kg and 7.8×10^9 kg, respectively, of high-temperature supercritical water and vapor supplied to the crust surrounding the conduit. These fluids in hydrothermal systems have the potential to form veins and disseminated mineral deposits within highly altered zones of wall rock surrounding conduits. Syneruptive inputs of magmatic volatiles, fluids and metals into the shallow (~500 m) subseafloor around conduits in deep submarine settings cannot be assigned into classical epithermal or porphyry-style mineralization models (e.g., Large, 1992; Sillitoe and Hedenquist, 2003). Hybrid-styles of epithermal-volcanic-hosted massive sulfide-porphyry deposition have been proposed for both active modern and ancient ore bodies, e.g., Mount Lyell (Yosemite, California; Huston and Kamprad, 2001) and Brothers volcano (South Pacific Ocean; Keith et al., 2018). Greater

204 understanding of these hybrid mineral systems could be attained by geothermal, chemical
205 and hydrological modeling constrained by quantitative information from Havre volcano.

206 **ACKNOWLEDGMENTS**

207 We thank the Mapping Exploration and Sampling of Havre (MESH) team,
208 remotely and autonomously operated vehicle operators, and the R/V *Roger Revelle* crew
209 for making this science possible. Manga was supported by National Science Foundation
210 (NSF) grant 1521855. Carey was supported by Australian Research Council Postdoctoral
211 fellowships (grants DP110102196 and DE150101190). Carey and Mitchell were
212 supported by NSF grants OCE1357443 and OCE1357216. SIMS analysis was funded by
213 Lipman Research Award GSA12295–18. We thank the reviewers for thoughtful
214 comments

215 **REFERENCES CITED**

216 Aravena, A., Cioni, R., de' Michieli Vitturi, M., Pistolesi, M., Ripepe, M., and Neri, A.,
217 2018, Evolution of conduit geometry and eruptive parameters during effusive events:
218 Geophysical Research Letters, v. 45, p. 7471-7480,
219 https://doi.org/10.2019/2018GL077806.
220 Befus, K.S., Manga, M., Gardner, J.E., and Williams, M., 2015, Ascent and emplacement
221 dynamics of obsidian lavas inferred from microlite textures: Bulletin of
222 Volcanology, v. 77, p. 88, https://doi.org/10.1007/s00445-015-0971-6.
223 Carey, R., et al., 2018, The largest deep-ocean silicic volcanic eruption of the past
224 century: Science Advances, v. 4, e1701121, https://doi.org/10.1126/sciadv.1701121.

225 Cassidy, M., Manga, M., Cashman, K.V., and Bachmann, O., 2018, Controls on
226 explosive-effusive volcanic eruption styles: Nature Communications, v. 9, p. 2839,
227 doi:https://doi.org/10.1038/s41467-018-05293-3.
228 Chevalier, L., Collombet, M., and Pinel, V., 2017, Temporal evolution of magma flow
229 and degassing conditions during dome growth, insights from 2D numerical
230 modeling: Journal of Volcanology and Geothermal Research, v. 333–334, p. 116–
231 133, https://doi.org/10.1016/j.jvolgeores.2017.01.016, erratum available at
232 http://dx.doi.org/10.1016/j.jvolgeores.2017.06.008.
233 Costa, A., Melnik, O., and Sparks, R.S.J., 2007, Controls of conduit geometry and
234 wallrock elasticity on lava dome eruptions: Earth and Planetary Science Letters,
235 v. 260, p. 137–151, https://doi.org/10.1016/j.epsl.2007.05.024.
236 Fauria, K.F., and Manga, M., 2018, Pyroclast cooling and saturation in water: Journal of
237 Volcanology and Geothermal Research, v. 362, p. 17–31,
238 https://doi.org/10.1016/j.jvolgeores.2018.07.002.
239 Fisher, A.T., 1998, Permeability within basaltic oceanic crust: Reviews of Geophysics,
240 v. 36, p. 143–182, https://doi.org/10.1029/97RG02916.
241 Giordano, D., Russell, J.K., and Dingwell, D.B., 2008, Viscosity of magmatic liquids: A
242 model: Earth and Planetary Science Letters, v. 271, p. 123–134,
243 https://doi.org/10.1016/j.epsl.2008.03.038.
244 Huston, D.L., and Kamprad, J., 2001, Zonation of alteration facies at western Tharsis:
245 implications for the genesis of Cu-Au deposits, Mount Lyell field, western
246 Tasmania: Economic Geology and the Bulletin of the Society of Economic
247 Geologists, v. 96, p. 1123–1132, https://doi.org/10.2113/gsecongeo.96.5.1123.

Jaupart, C., and Allègre, C.J., 1991, Gas content, eruption rate and instabilities of eruption regime in silicic volcanoes: Earth and Planetary Science Letters, v. 102, p. 413–429, https://doi.org/10.1016/0012-821X(91)90032-D.

Jutzeler, M., Marsh, R., Carey, R.J., White, J.D.L., Talling, P.J., and Karlstrom, L., 2014, On the fate of pumice rafts formed during the 2012 Havre submarine eruption: Nature Communications, v. 5, p. 3660, https://doi.org/10.1038/ncomms4660.

Keith, M., Haase, K.M., Klemd, R., Smith, D.J., Schwarz-Schampera, U., and Bach, W., 2018, Constraints on the source of Cu in a submarine magmatic-hydrothermal system, Brothers volcano, Kermadec island arc: Contributions to Mineralogy and Petrology, v. 173, p. 40, https://doi.org/10.1007/s00410-018-1470-5.

Kozono, T., and Koyaguchi, T., 2012, Effects of gas escape and crystallization on the complexity of conduit flow dynamics during lava dome eruptions: Journal of Geophysical Research. Solid Earth, v. 117, B08204, https://doi.org/10.1029/2012JB009343.

Large, R.R., 1992, Australian volcanic-hosted massive sulfide deposits: Features, styles, and genetic models: Economic Geology and the Bulletin of the Society of Economic Geologists, v. 87, p. 471–510, https://doi.org/10.2113/gsecongeo.87.3.471.

Llewellin, E.W., and Manga, M., 2005, Bubble suspension rheology and implications for conduit flow: Journal of Volcanology and Geothermal Research, v. 143, p. 205–217, https://doi.org/10.1016/j.jvolgeores.2004.09.018.

Manga, M., et al., 2018, The pumice raft-forming 2012 Havre submarine eruption was effusive: Earth and Planetary Science Letters, v. 489, p. 49–58, https://doi.org/10.1016/j.epsl.2018.02.025.

271 Manning, C.E., and Ingebritsen, S.E., 1999, Permeability of the continental crust:
272 Implications of geothermal data and metamorphic systems: Reviews of Geophysics,
273 v. 37, p. 127–150, https://doi.org/10.1029/1998RG900002.
274 Mitchell, S.J., McIntosh, I.M., Houghton, B.F., Carey, R.J., and Shea, T., 2018,
275 Dynamics of a powerful deep submarine eruption recorded in H_2O contents and
276 speciation in rhyolitic glass: The 2012 Havre eruption: Earth and Planetary Science
277 Letters, v. 494, p. 135–147, https://doi.org/10.1016/j.epsl.2018.04.053.
278 Mueller, S., Melnik, O., Spieler, O., Scheu, B., and Dingwell, D.B., 2005, Permeability
279 and degassing of dome lavas undergoing rapid decompression: An experimental
280 determination: Bulletin of Volcanology, v. 67, p. 526–538,
281 https://doi.org/10.1007/s00445-004-0392-4.
282 National Academies of Sciences, Engineering, and Medicine, 2017, Volcanic eruptions
283 and their repose, unrest, precursors, and timing: Washington, D.C., National
284 Academies Press, 122 p.
285 Pallister, J.S., Diefenbach, A.K., Burton, W.C., Muñoz, J., Griswold, J.P., Lara, L.E.,
286 Lowenstern, J.B., and Valenzuela, C.E., 2013, The Chaitén rhyolite lava dome:
287 Eruption sequence, lava dome volumes, rapid effusion rates and source of the
288 rhyolite magma: Andean Geology, v. 40, p. 277–294,
289 https://doi.org/10.5027/andgeoV40n2-a06.
290 Rotella, M.D., Wilson, C.J., Barker, S.J., Schipper, C.I., Wright, I.C., and Wysoczanski,
291 R.J., 2015, Dynamics of deep submarine silicic explosive eruptions in the Kermadec
292 arc, as reflected in pumice vesicularity textures: Journal of Volcanology and

293 Geothermal Research, v. 301, p. 314–332,
294 https://doi.org/10.1016/j.jvolgeores.2015.05.021.
295 Schipper, C.I., Castro, J.M., Tuffen, H., James, M.R., and How, P., 2013, Shallow vent
296 architecture during hybrid explosive–effusive activity at Cordón Caulle (Chile,
297 2011–12): Evidence from direct observations and pyroclast textures: Journal of
298 Volcanology and Geothermal Research, v. 262, p. 25–37,
299 https://doi.org/10.1016/j.jvolgeores.2013.06.005.
300 Schipper, C.I., Mandon, C., Maksimenko, A., Castro, J.M., Conway, C.E., Hauer, P.,
301 Kirilova, M., and Kilgour, G., 2017, Vapor-phase cristobalite as a durable indicator
302 of magmatic pore structure and halogen degassing: an example from White Island
303 volcano (New Zealand): Bulletin of Volcanology, v. 79, p. 74,
304 https://doi.org/10.1007/s00445-017-1157-1.
305 Sillitoe, R.H., and Hedenquist, J.W., 2003, Linkages between volcanotectonic settings,
306 ore-fluid compositions, and epithermal precious metal deposits, *in* Simmons, S.F.,
307 and Graham, I.J., eds., Volcanic, geothermal, and ore-forming fluids: Rulers and
308 witnesses of processes within the Earth: Society of Economic Geologists Special
309 Publication, v. 10, p. 315–343.
310 Tuffen, H., James, M.R., Castro, J.M., and Schipper, C.I., 2013, Exceptional mobility of
311 an advancing rhyolitic obsidian flow at Cordón Caulle volcano in Chile: Nature
312 Communications, v. 4, p. 2709, https://doi.org/10.1038/ncomms3709.
313 van Otterloo, J., Cas, R.A., and Scutter, C.R., 2015, The fracture behaviour of volcanic
314 glass and relevance to quench fragmentation during formation of hyaloclastite and

phreatomagmatism: Earth-Science Reviews, v. 151, p. 79–116, https://doi.org/10.1016/j.earscirev.2015.10.003.

Woods, A.W., and Koyaguchi, T., 1994, Transitions between explosive and effusive eruptions of silicic magmas: Nature, v. 370, p. 641, https://doi.org/10.1038/370641a0.

FIGURES

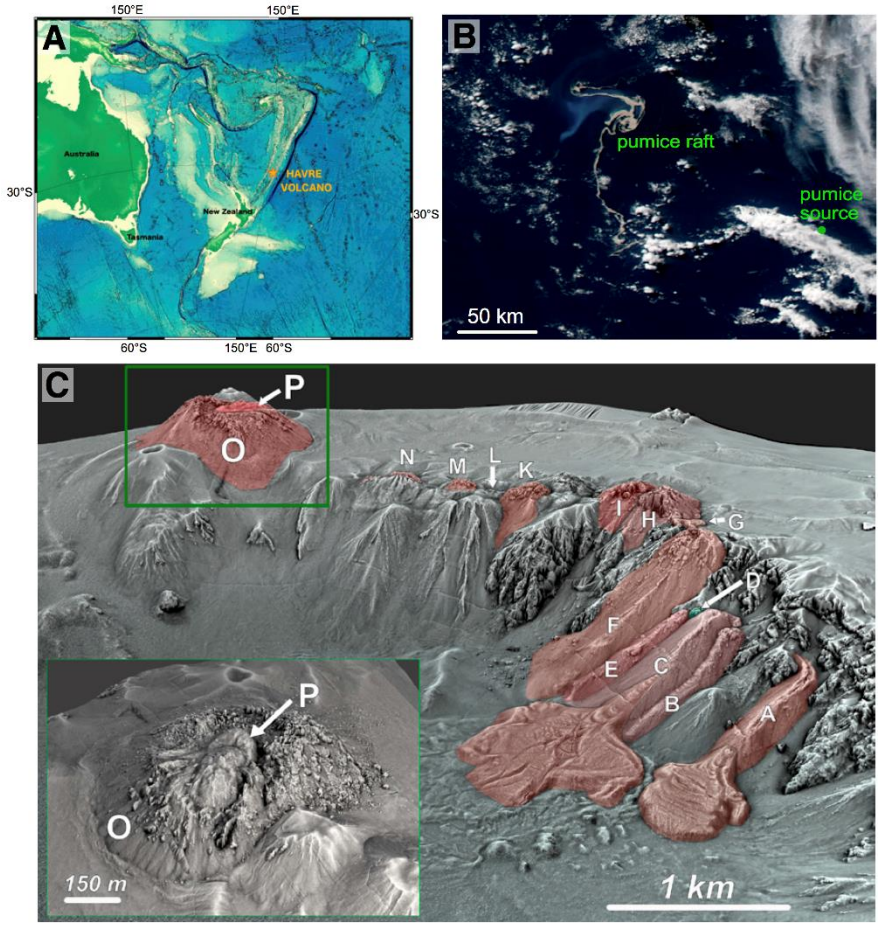

Figure 1. A: Location of the Havre volcano in the Kermadec arc, South Pacific Ocean. B: Image of pumice raft, 5 d after eruption. C: Map of caldera identifying newly erupted lava flows and domes in red (lettered).

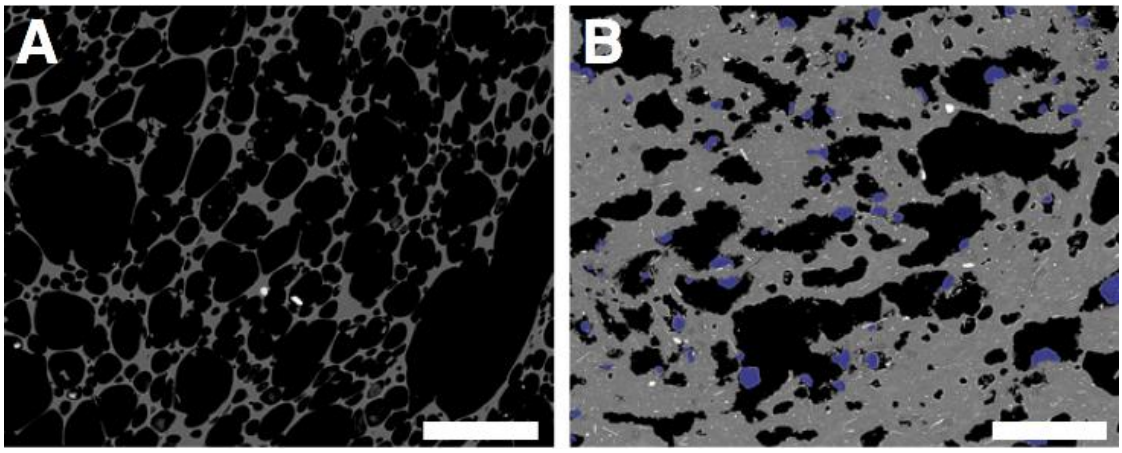

Figure 2. Backscatter electron images of representative clast texture from (A) the raft and (B) the dome. In B cristobalite is colored blue. Microlites of plagioclase (white) and pyroxene (dark gray) dominate the groundmass in B. Vesicularities are 83 vol% in A and 34.5 vol% in B. Bar in the lower right is 100 μm long.

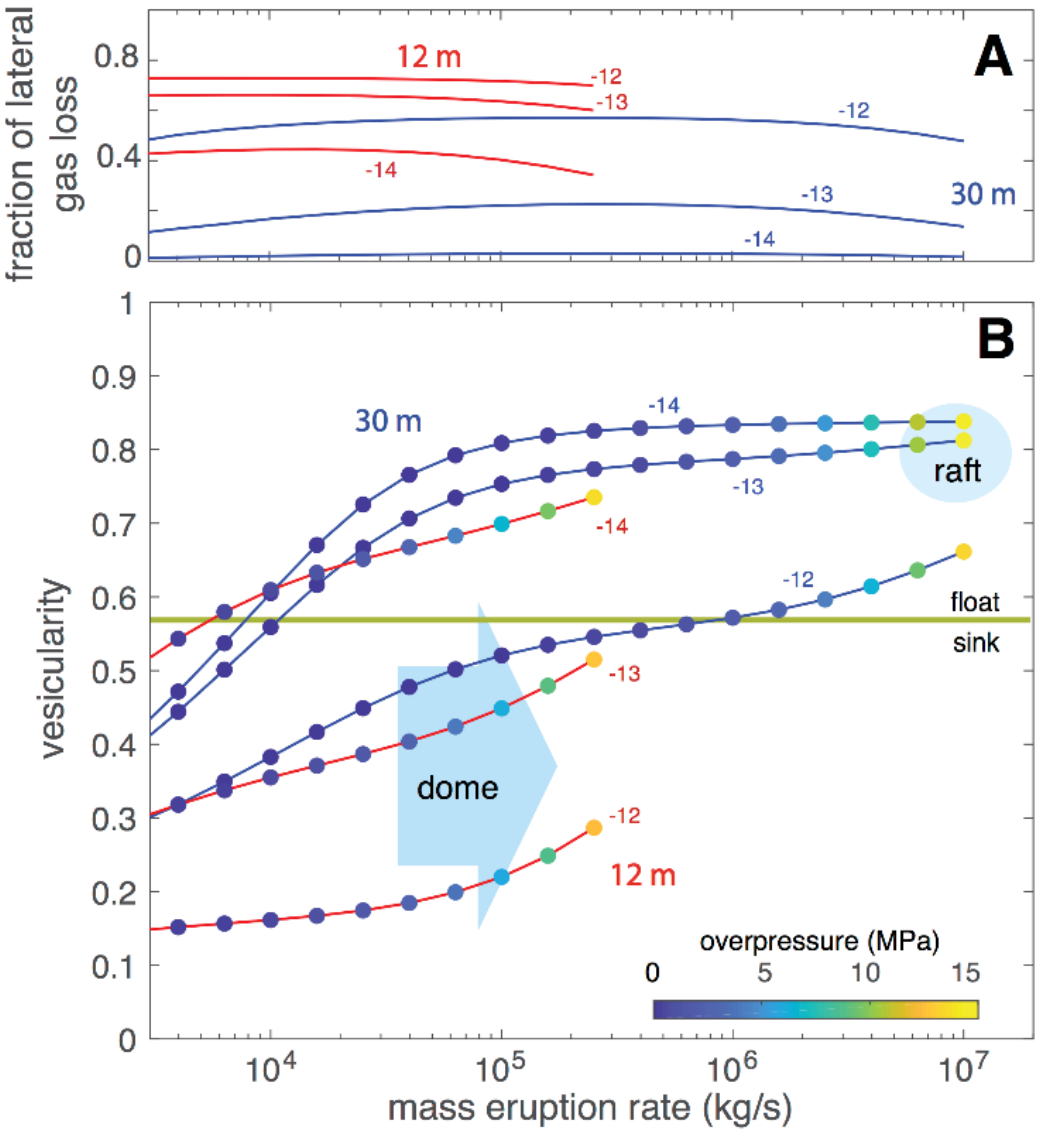

Figure 3. A: Fraction of initial total dissolved water lost to country rocks during ascent. B: Relationship between mass eruption rate and vesicularity at vent. Blue and red curves indicate conduit radii of 30 and 12 m, respectively. Colors of symbols show overpressure at base of conduit (5 km below seafloor). Horizontal line shows vesicularity needed for clasts to be buoyant prior to ingesting liquid water. In A and B, numbers next to each curve are $\log_{10}$ of permeability (in m^2).

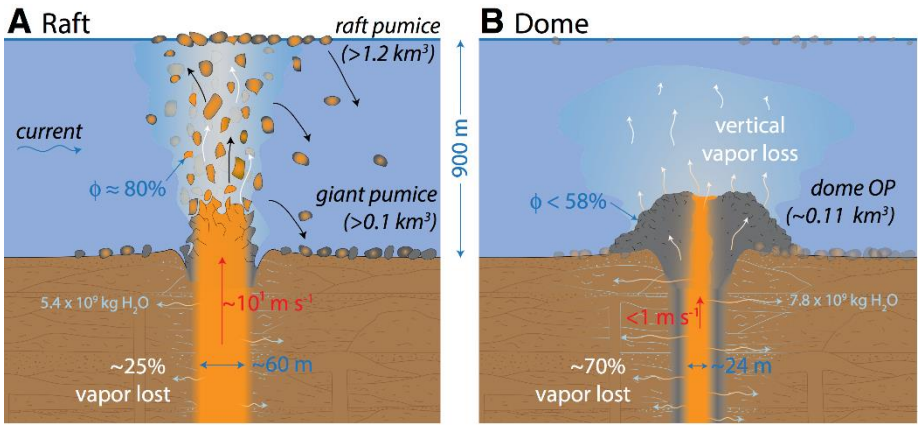

Figure 4. Cartoon illustrating the dynamics that accompanied (A) pumice raft-forming eruptions and (B) dome-forming eruptions at Havre volcano (southwest Pacific Ocean) in 2012. Subsurface structure is schematic; ϕ is gas volume fraction.

Supplementary material contains Tables DR1-DR4 and Figure DR5. See online publication.